Real-Time Rendering of Indirectly Visible Caustics

Pierre Moreau[a], Michael Doggett[b]
Faculty of Engineering, Lund University, Lund, Sweden
{pierre.moreau, michael.doggett}@cs.lth.se

Keywords: Real-time, Ray tracing, Caustics rendering

Abstract: Caustics are a challenging light transport phenomenon to render in real-time, and most previous approaches have used screen-space accumulation based on the fast rasterization hardware of GPUs. This limits the position of photon collection points to first hit screen space locations, and leads to missing caustics that should be visible in a mirror's reflection. In this paper we propose an algorithm that can render caustics visible via specular bounces in real-time. The algorithm takes advantage of hardware-accelerated ray tracing support found in modern GPUs. By constructing an acceleration structure around multiple bounce view ray hit points in world space, and tracing multiple bounce light rays through the scene, we ensure caustics can be created anywhere in the scene, not just in screen space. We analyze the performance and image quality of our approach, and show that we can produce indirectly visible caustics at real-time rates.

Presented at GRAPP 2022
https://grapp.scitevents.org/Home.aspx/?y=2022
DOI: 10.5220/0010777800003124

1 INTRODUCTION

Caustics are a natural phenomenon created by the concentration of light as it is reflected and transmitted through objects. While many techniques exist to generate these lighting effects in images of three dimensional scenes, generating them in real-time for interactive applications is challenging. A popular approach to achieving real-time performance is the use of screen-space algorithms, but these algorithms come with limitations, in particular not working well for scenes with reflective surfaces and semi-transparent objects. For consistent viewing of rendered images, lighting effects like caustics need to remain constant. Screen-space accumulation techniques can lead to inconsistent renderings with lighting effects switching on and off, or even missing in mirrors, as can be seen in Figure 1 for the technique by Kim (2019).

[a] https://orcid.org/0000-0003-3916-1250
[b] https://orcid.org/0000-0002-4848-3481

Caustics have always been an important feature of rendering research and go back to early backward ray tracing techniques (Arvo, 1986). More recent approaches have used the rasterization pipeline and off-screen buffers for a range of techniques such as caustic mapping (Hu and Qin, 2007; Shah et al., 2007; Szirmay-Kalos et al., 2005; Wyman and Davis, 2006). While these techniques create good approximations, many issues remain, including sampling rates, large numbers of photons, and potential coherency problems during animation. With the recent introduction of hardware-accelerated ray tracing, new approaches (Kim, 2019; Ouyang and Yang, 2020a; Yang and Ouyang, 2021) take advantage of this to create high-quality caustics, but still do not handle caustics not directly visible.

Screen-space accumulation techniques that only collect lighting contributions at locations that are directly visible by the current camera are always limited in terms of correctly rendering a scene. For the case of a scene where a caustic is visible via its reflection in a mirror, the lighting contributions would be collected on the mirror itself. This means the photons responsible for the caustic would need to be reflected off the diffuse surface and into one of the collection locations on the mirror. This is unlikely as the BSDF sampling will have a low chance at returning a direction towards the mirror in most cases and that direction needs to be within the tight lobe of a rough mirror, and outright impossible in the case of

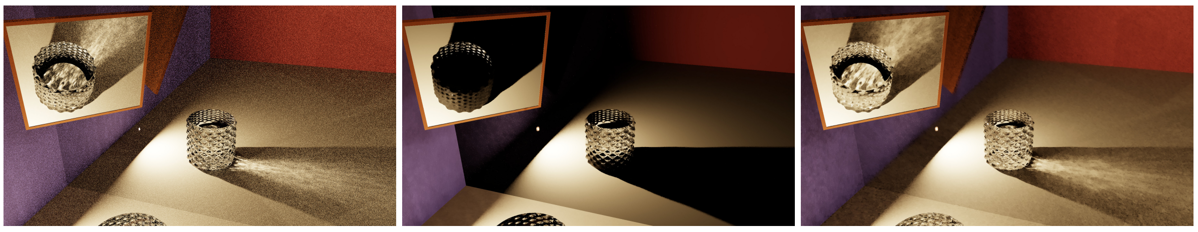
(a) Reference (b) Kim (2019), 24.7 ms (c) Our approach, 25.6 ms

Figure 1: This figure shows a challenging setup for real-time caustics which are only visible via a chain of specular events, such as mirror reflections. As Kim (2019) accumulates photon contributions in screen space, contributions for anything seen via this perfectly specular mirror will be collected on the mirror itself requiring them to come from one very specific direction in order to have any impact; the caustics visible via the different mirrors are completely missing as a result. Our new approach can handle the caustics since its accumulation is based around a world-space acceleration structure. This scene was rendered at 1920×1080 with a path length of 6 segments using different algorithms; (a) uses 125k *samples per pixel* (spp), (b) 1 spp and 14M light paths, and (c), our temporal approach, 1 spp and 1M light paths.

a perfectly-specular mirror. Furthermore most real-time caustic-rendering techniques stop the light path at the first diffuse hit, preventing the caustic photons from ever reaching that mirror and being accounted for; this cut is performed for performance reasons as caustic paths with two or more diffuse hits will have a more subtle contribution than caustic paths with a single diffuse hit.

This paper proposes to collect photons, on diffuse surfaces, at viewing ray hit points, found using hardware-accelerated ray tracing. At each hit point for a light path, a Bounding Volume Hierarchy (BVH) node is created and constructed into a BVH tree using DirectX Raytracing. By creating a full scene BVH, the algorithm is not limited to screen-space- or view-frustum-based images. We then query the BVH using the algorithm by Evangelou et al. (2021). We also use ray differentials for appropriate sizing of the BVH nodes, and use the BVH structure as a temporal cache for filtering. Our key contribution is enabling real-time indirect caustics, by combining view and light rays with a custom BVH, all using ray tracing hardware acceleration.

2 RELATED WORK

Tracing light rays or photons from a light source to an opaque surface and accumulating light intensity on a surface has been a common approach to generating caustics (Arvo, 1986; Jensen, 2001). Generating caustics in real-time can be done by reproducing photon mapping on a GPU (McGuire and Luebke, 2009), but these approaches are expensive and not capable of generating highly accurate caustics.

Another method for generating caustics in real-time is caustic maps. Caustic maps are generated by first making a photon buffer by emitting photons from the light's perspective into a two-dimensional buffer similar to shadow maps. The photons from the photon buffer are then drawn into the caustic map, which is projected onto the final image. Szirmay-Kalos et al. (2005) and Wyman and Davis (2006) improved quality by increasing photon count and Wyman and Nichols (2009) created a hierarchical caustic map, that adaptively processed only the necessary parts of the photon buffer. But caustic maps still limit the locations that photons can be captured at, and the projection of high photon counts into the caustic map quickly becomes expensive when trying to improve image quality.

With the advent of hardware accelerated ray tracing, several new approaches to real-time rendering of caustics have made use of this feature. Kim (2019) uses projection volumes to direct photons towards semi-transparent objects to create photon maps limiting visible caustics to these projection volumes. Gruen (2019) focuses on creating volumetric water caustics in single-scattering participating media where a water surface casts a caustic on an underlying surface, but it does not handle refracted and then reflected light rays. Ouyang and Yang (2020a,b); Yang and Ouyang (2021) introduce caustic meshes for general caustics, but their method requires two passes for reflected and refracted caustics, and only caustics in the current viewport can be seen in this case. They further combine their technique with cascaded caustic maps for water caustics, but are focused on the caustic on the surface underlying the water. Wang and Zhang (2021) only trace rays after intersecting with a semi-transparent object, at which point it fires photons into a caustic map to layer onto the final image. By using a caustic map, their algorithm has similar limitations to screen-space techniques. While all these recent methods address caustics, some are screen space limited, and none of them address the issues of indirect caustics where photons must be accumulated outside the view frustum to correctly handle reflected caustics, and caustics behind semi-transparent objects.

Evangelou et al. (2021) present a fast radius search by mapping the problem to GPU ray traversal and can therefore take advantage of ray tracing hardware. In our algorithm, we utilise their approach to query the BVH used when accumulating photons as well as when reusing the accumulation results in later frames. They evaluate their algorithm by using it for progressive photon mapping (Hachisuka et al., 2008) by building an acceleration structure around the photons traced from the light, whereas in our algorithm we build the acceleration structure around the camera ray hit points, where photons are collected.

3 ALGORITHM

Unlike screen-space techniques, our approach accumulates photons in a world-space caching structure based on arbitrary points and their surroundings. The size of that area is uniquely computed at each caching point, enabling support for fine-detail caustics.

The stages of our algorithm are shown in Figure 2. The first stage is a path tracer which identifies the first diffuse hit found along each camera path where light contributions will later be collected, similar to *progressive photon mapping* (Hachisuka et al., 2008). In our algorithm we refer to these *hit points* as *collection points*. An acceleration structure is then created around the collection points, and light paths are traced to accumulate light intensity at each collection point. Finally the output is resolved before being processed using a spatiotemporal filter.

We will be using the following notation: c_i refers to a collection point in frame i, $\mathbf{C}_i$ refers to all collection points present in frame i. A collection point has the following attributes:

p	world position
τ	camera sub-path throughput
r	search radius
n	world normal
I	accumulated radiant intensity
m	material ID
L_o	exitant radiance
$\tilde{L}_o$	interpolated exitant radiance
$\hat{L}_o$	weighted contributions from previous collection points

Figure 3 shows an overview of our setup with camera and light paths. When path tracing, the collection points are selected based on the BSDF component that was evaluated for generating the reflected ray at a hit: if a diffuse component was used, then we create a collection point at the hit point. In Figure 3, this is the case for p_1 and m_2 but not m_1 as it sampled the specular component of the mirror.

Selecting a search radius. As collecting from a single point in space is infeasible in practice, we instead gather from a surrounding area. We use the radius of the disk enclosing the pixel footprint in world space for the collection points at primary hits, as a reasonable middle ground between over-blurring and light leakage, and too restrictive radii that would ignore most light paths.

To compute the pixel footprint for collection points at secondary hits, we use half the width of ray cones as described by Akenine-Möller et al. (2021) as our search radius, and take the BSDF roughness into account as described in their Section 4. The ray cones computation is cheaper than ray differentials (Igehy, 1999), and is necessary for texture level of detail calculation.

Creating the acceleration structure. We use a similar approach to Evangelou et al. (2021) for accelerating radius searches. In their work they recommended building the acceleration structure around the photons rather than around the collection points, as atomics can then be avoided for updating the accumulated contributions at each collection point, as having overlapping collection points (for example when the same area is visible both directly and via a mirror) can noticeably decrease performance. The overhead from using atomics is about 5%; please see Section 3.2 for more details.

In contrast, we build the acceleration structure around the collection points for the following reasons:

- more predictable quality reduction when decreasing the number of collection points to improve performance, than reducing the number of photons stored;
- the light contributions accumulated at collection points can be easily reused over multiple frames, as presented in Section 3.1.
- building around photons forces the use of the largest radius for each of them, which can be costly as radii depend on location and intersected shapes and materials;

As numerical precision errors might result in the hit position being slightly above or below the surface, we gather from a cylinder rather than from a disk, similarly to most photon mapping methods. The cylinder is aligned along $c_i.n$, uses the same radius $c_i.r$, and has its height set to a tenth of $c_i.r$. We then compute the smallest AABB containing that cylinder

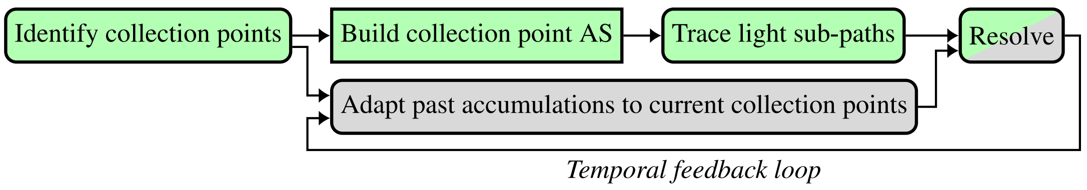
Identify collection points
Build collection point AS
Trace light sub-paths
Resolve
Adapt past accumulations to current collection points
Temporal feedback loop

Figure 2: An overview of the different steps of our approach, with all boxes with a green colour constituting the basic algorithm, and the grey ones were either added or modified to support temporal reuse. All steps are performed in programmable shaders, except for the rectangle with non-rounded corners, which is instead taken care of by the API.

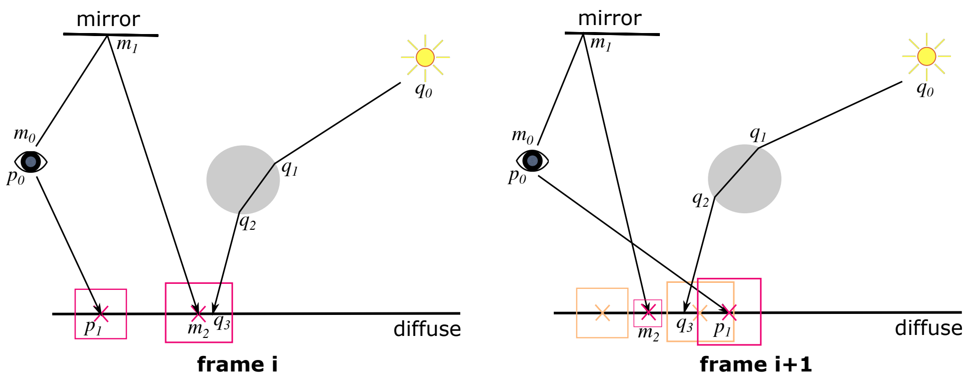

Figure 3: An overview of our indirect-caustic algorithm. Camera paths, *p, m*, are traced to the first diffuse surface intersection, where collection points (shown as red boxes) are created and placed in a BVH. Then light paths, *q*, are traced via specular intersections and collected. The path *m* will generate an indirect caustic in the final image. On the right half of the image is frame $i+1$, which shows how new collection points are created when the camera rays change, but collection points from previous frames can still be reused.

and use it as the primitive around which the acceleration structure is built.

Tracing light sub-paths. The algorithm does not depend on how the set of light sources and individual light sources are being sampled, so different techniques can be used here such as the recent works by Kim (2019) or by Ouyang and Yang (2020a); Yang and Ouyang (2021).

Regardless of the chosen method(s) for sampling and tracing the light sub-paths, every time the sub-path hits a surface we will query and selectively update all collection points that contain this hit. As we leverage a hardware accelerated BVH and ray tracing API, this is implemented by tracing a very short ray (Wald et al., 2019), starting from the hit, against the acceleration structure storing our collection points. For each intersected collection point, we first check that the hit is actually located within the collection cylinder and that its material identifier matches the one stored in the collection point, before accumulating in $c_i.I$ the flux carried by the photon into radiant intensity reflected towards the vertex prior to the collection point in the camera sub-path (e.g. towards m_1 if accumulating at m_2).

Resolving. Before presenting the results to the user, the accumulated radiant intensity needs to be transformed into radiance, and take account of the throughput of the camera sub-path connecting a collection point to a pixel. This is summarised in the following equation:

$$c_i.L_o = c_i.\tau \frac{c_i.I}{\pi c_i.r^2} \tag{1}$$

3.1 Temporal Reuse

A benefit of our approach is that we can reuse the exact same accumulated radiant intensity and just multiply it by the new camera sub-path throughput when a directly-visible caustic moves behind a transparent object for example, as only the light sub-path contribution gets accumulated. Whereas this accumulated data would usually be discarded by filters on occlusions or disocclusions, having the data stored in world space allows us to reuse it if appropriate.

The reuse happens in two separate steps: first we gather contributions from all past collection points located near current ones, and second, past and present contributions are combined together during the resolve step using an exponential moving average with

$\alpha = 0.8$:

$$c_i.\tilde{L}_o = \alpha c_i.\hat{L}_o + (1-\alpha)c_i.L_o \tag{2}$$

Reusing past accumulations. This takes place between the identification of collection points in the current frame and resolve. If keeping two acceleration structures in memory is an issue, this step should be performed before updating the collection point acceleration structure for the current frame.

We query all collection points $c_{i-1} \in \mathbf{C}_{i-1}$ containing $c_i.p$, by tracing a very short ray originating from $c_i.p$ against the acceleration structure built during the previous frame. For each intersected collection point c_{i-1} satisfying the system of equations (4) (similar to a bilateral filter), its interpolated radiance $c_{i-1}.\tilde{L}_o$ weighted by a Gaussian kernel $w(c_{i-1})$ of width $\sigma = \frac{3}{4}c_i.r$ is accumulated into $c_i.\hat{L}_o$:

$$w(c_{i-1}) = \exp\left(\frac{-\|c_i.p - c_{i-1}.p\|^2}{2\sigma^2}\right) \tag{3}$$

$$\begin{cases} \|c_{i-1}.p - c_i.p\| \leq c_i.r \\ c_{i-1}.n \cdot c_i.n \geq 0.9 \\ c_{i-1}.m = c_i.m \end{cases} \tag{4}$$

3.2 Implementation Details

General constraints. If path tracing is used by an application, care needs to be taken to avoid the path tracer evaluating the same paths as the photon-based approach, or to weigh them appropriately. As we simply add the results from both approaches, we prevent the path tracer from evaluating paths containing at least one diffuse and one specular bounce as those will be handled by the photon-based approach. Using Heckbert's light transport notation (Heckbert, 1990), this corresponds to paths of the form ES*D(S|D)*S(S|D)*L.

In all presented results, the search radius was capped to 5 mm as a middle ground between performance of the light tracing stage and quality.

Performance improvements. For the first stage of the pipeline, we found that storing all the data associated to our caching approach as soon as a suitable collection point was identified, rather than at the end to minimise control flow divergence, improved the performance of that stage from 20 ms down to about 4 ms. This is due to not having to keep all that data live accross the tracing of path segments.

As current APIs do not expose atomic additions for floats, we first implemented the contribution accumulation using atomic compare-and-swap within a loop, resulting in a 15% overhead compared to no atomics. By instead using fixed-point values and integer atomic add, the overhead was reduced to 5%. As the accumulated values are well below 1, we only used 4 digits for the decimal part and the remaining 28 for the fractional part.

4 RESULTS

We implemented our approach on top of Kim's (2019), inside the Falcor (Benty et al., 2020) 4.3 framework using the DirectX 12 and DirectX Raytracing API. All results were obtained on an NVIDIA Geforce RTX 3080 with NVIDIA's 471.96 drivers, and rendered at 1920×1080 with a maximum path length of 6 segments and using 1024^2 light paths, unless mentioned otherwise. *Spatiotemporal Variance-Guided Filtering* (SVGF) (Schied et al., 2017) was used to filter the computed images before presenting them to the user.

In the following section we will be using the following abbreviations for methods: *OurBasic* which refers to our basic algorithm described in Section 3 (i.e. without the temporal component) and integrated with a path tracer as described in Section 3.2, and *OurTemporal* which is our full algorithm (i.e. *OurBasic* plus the temporal component described in Section 3.1).

All scenes, besides the ones shown in Figure 7, use a similar template of a closed box whose left and back wall and ceiling are specular, with the other parts being diffuse. This box contains a simple emissive mesh as the only light source, a transparent object, and a mirror. Of these scenes, four have animations of different types: *a*nimated *c*amera (AC), *a*nimated *l*ight (AL), *a*nimated *g*eometry (AG; it is the transparent sphere), and *a*ll *a*nimated (AA; it combines all previous animations). They are all 10 seconds long and animated at 30 fps. Unless mentioned otherwise, the specular walls and ceiling in the animated scenes have a roughness R of 0.08.

The *Bistro Exterior* and *Bistro Interior* scenes used in Figure 7 were modified to limit the number of emissive triangles by setting the emissivity to 0 for most light sources. Additionally in *Bistro Interior*, light paths were only traced from the lamps placed on tables. To more easily showcase caustics, transparent objects were added on the tables in *Bistro Exterior* while some of the glasses were removed from *Bistro Interior* to make more room on the tables. In both scenes, the windows of the bistro were changed from a very rough glossy surface into a specular mirror.

The source code and the videos can be found on

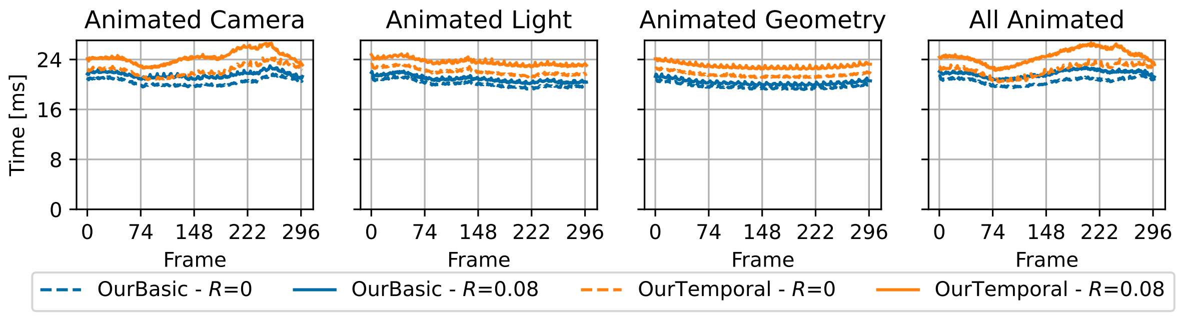

Figure 4: Measuring the total frame time taken by our basic and temporal algorithms for different types of animations. For comparison a path tracer at equal quality would require about 175 spp and take between 2.5 and 3 seconds; this was measured for equal ꟻLIP-mean on AC@150 and AC@298.

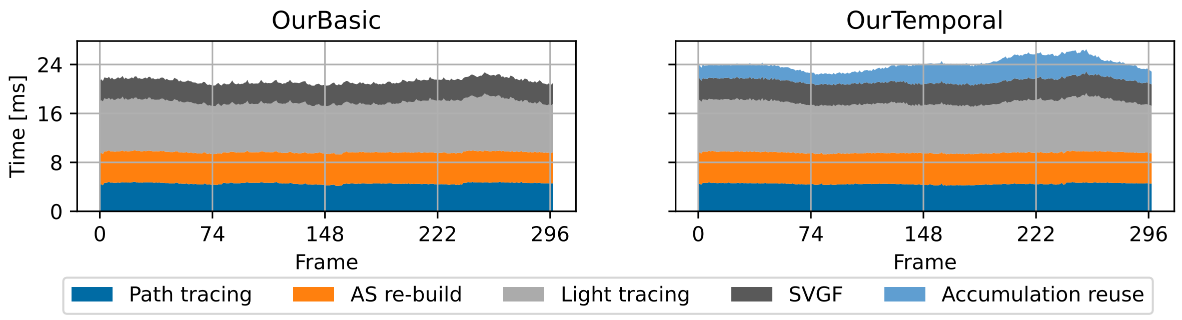

Figure 5: Highlighting the performance of the main stages of the algorithm during the animation in the scene AC. The identification of collection points is performed during the path tracing step, and the G-buffer generation time (a constant 0.6 ms) was also included under the *Path tracing* step, while the *resolve* stage (a constant 0.4 ms) was included under the *SVGF* step. 90% of the re-build time is spent on the bottom level acceleration structure. Not part of these plots, there is an additional 0.27 ms per frame from tonemapping and other miscellaneous operations to reach the timings presented in Figure 4. Note that *accumulation reuse* could be run concurrently to re-building the acceleration structure and tracing the light paths.

the project page[1].

4.1 Performance

To evaluate the performance of our approach, we ran it on different types of animations to see their impact.

Looking first at the total frame times presented in Figure 4, we can see that the cost of our approaches remains relatively constant throughout the light and geometry animations. Larger changes can be observed during the camera animation and seem to mostly correspond to changes in the number of bounces before hitting a diffuse surface from the camera. Most of that time variation comes from the pass reusing the accumulated contributions from previous frames with the current collection points.

Our approach can extend current path tracing-based frameworks and as such reuse some of the computations already performed there. For example the identification of collection points can be added to an existing path tracer to store additional data without having to re-trace the same rays in a separate pass. We noted an increase in the cost of that pass from about 3 ms to about 4 ms when doing so, for a path tracer ignoring caustic paths. This combined cost is presented in Figure 5, along with the cost of the other steps.

The largest part of the cost of *accumulation reuse* and *light tracing* comes from tracing against the collection point acceleration structure and the invocation of the intersection and any-hit shader, due to overlapping collection points and memory accesses to get the needed information during the evaluation of the shaders. For comparison, the same light tracing but with the accumulation performed in screen space as presented by (Kim, 2019) takes 1–1.5 ms, as opposed to the 8.5–9 ms of our approach.

The second most expensive step is rebuilding the acceleration structure. Rebuilding remains an expensive operation for any real-time ray tracing-based workflow, and as such refitting is favoured for

[1]https://fileadmin.cs.lth.se/graphics/research/papers/2022/indirectly_visible_caustics/

Table 1: Average image quality measurements over 10 iterations using SVGF. OurBasic performing slightly better than OurTemporal after filtering in AL@150 can be explained by both the temporal lag and the contribution of longer paths having a larger impact on the final image than in the other scenes. *Equal Time PT (3 spp)* is about the same time as, or slightly more expensive than, OurTemporal. The standard deviation was at or below 3.7% of the mean in all configurations, except for the filtered output in AG@10 for *OurTemporal* which reached 12.7% of the mean.

Scene, FrameID	Measure	Equal Time PT (3 spp)		OurBasic		OurTemporal	
		Unfiltered	Filtered	Unfiltered	Filtered	Unfiltered	Filtered
Animated Camera,	MAE	0.074	0.041	0.084	0.022	0.065	**0.021**
Frame 150	ꟻLIP	0.335	0.292	0.280	0.190	0.241	**0.168**
Animated Camera,	MAE	0.162	0.063	0.150	0.036	0.111	**0.028**
Frame 298	ꟻLIP	0.468	0.363	0.410	0.229	0.309	**0.179**
Animated Light,	MAE	0.117	0.084	0.116	**0.037**	0.088	0.045
Frame 150	ꟻLIP	0.562	0.520	0.384	**0.273**	0.335	0.276
Animated Light,	MAE	0.077	0.034	0.097	0.029	0.073	**0.025**
Frame 298	ꟻLIP	0.323	0.292	0.338	0.261	0.291	**0.218**
Animated Geometry,	MAE	0.127	0.090	0.135	0.036	0.093	**0.034**
Frame 10	ꟻLIP	0.465	0.406	0.364	0.204	0.266	**0.173**
All Animated,	MAE	0.077	0.033	0.096	0.020	0.077	**0.019**
Frame 298	ꟻLIP	0.228	0.163	0.233	0.110	0.189	**0.093**

most frames while rebuilding can be performed asynchronously every now and then to keep the tracing performance optimal. However the location or distribution of collection points seemed to vary too much between frames, resulting in refitting degrading the tracing performance by an order of magnitude as soon as enabled. As the number of collection points depends on the resolution of the rendering and not on the scene, the cost of this step remained the same in the *Bistro Interior* and *Bistro Exterior* scenes from Figure 7.

4.2 Quality

As our approach targets real-time applications with different types of motions, we evaluated the quality at different points during animations rather than on still images. We looked at the quality both prior and after filtering, as well as both numerical (using *mean-absolute error* (MAE)) and perceptual (using ꟻLIP (Andersson et al., 2020)) methods; all measurements were performed on non-tonemapped outputs.

From Table 1 we can see that both *OurBasic* and *OurTemporal* improve for both metrics in all but one scene compared to the baseline. *OurTemporal* further improves compared to our basic algorithm in most scenes, for example in AC@198 the ꟻLIP results are improved by nearly 15%) but also presents some regressions as can be seen in AG@10 for example (though they are within run to run variance).

There are multiple reasons for those regressions that can be illustrated with results from Table 2. First, when we reuse accumulated radiance from previous frames we do not know the length of the light subpaths having contributed, so we can end up creating longer paths than what was specified, as can be seen for AG@10 in Table 2 at the top of the image where the mirror contains a reflection of the caustic on the ground, but that caustic is missing from the reference. This can be seen as an advantage, as longer paths can be created at no additional cost. A second one, which can be seen in the caustic in AA@298 for *OurTemporal*, is ghosting artefacts due to the temporal reuse simply relying on an exponential moving average; *Equal time PT* and *OurBasic* also suffer from some ghosting introduced by SVGF, but it is not as noticeable. Finally, there is a conflict between the two temporal reuse methods, our reuse at the collection points and the SVGF's one: as new regions become visible, our temporal reuse will end up creating two different noise levels for a given surface (the more converged one, which was visible for several frames, and the newly uncovered one with very few samples) which will be interpreted by SVGF as two different regions making them more visually distinct.

Another important note is that SVGF relies on motion vectors which are rarely readily available for light patterns such as caustics or shadows, or reflections or refractions, all of which are found all over these scenes. A recent approach by Zeng et al. (2021) shows promise regarding glossy reflections.

Temporal stability is sometimes improved in real-time applications by performing the filtering *after* tonemapping rather than *before*, though at the cost of image quality. This can however result in different samples being merged together due to no longer appearing distinct enough to the filter, such as the few caustic samples in the second picture of Figure 6

Table 2: Highlighting different scenarios: AC@298 where *OurTemporal* improved significantly compared to *OurBasic*, AG@10 presents a regression for *OurTemporal*, and AA@298 with an easier to sample caustic for the path tracer. For each scene, the first row consists of a single frame filtered with SVGF, whereas the second row has error maps generated by ꟻLIP (Andersson et al., 2020).

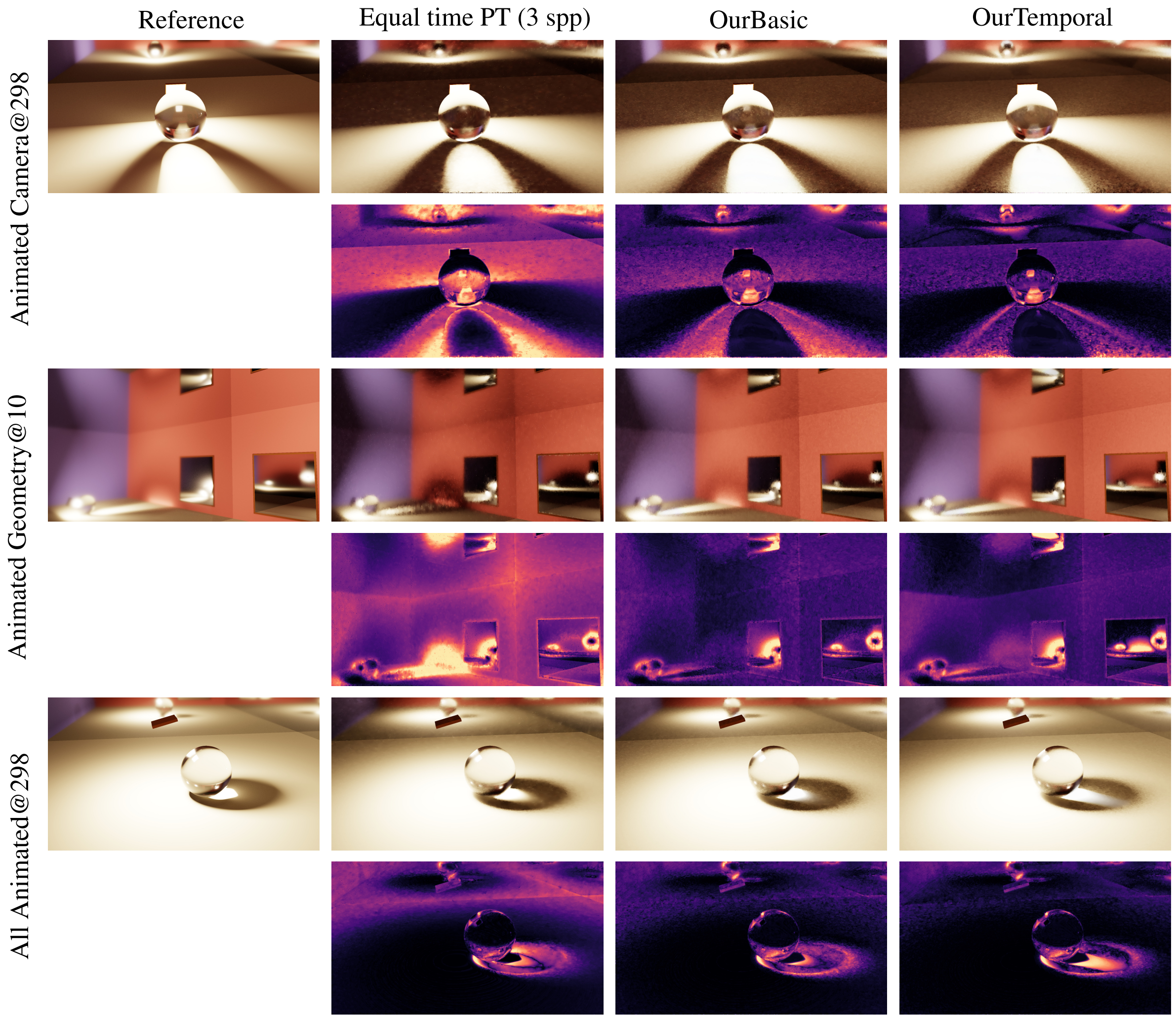

which were mostly blurred out. Thanks to our approach providing more samples, it can be used along that filtering trick.

Apart from the previously-mentioned ghosting in *OurTemporal*, the temporal quality depends strongly on the light sampling algorithm used and better results could be obtained with Ouyang and Yang (2020a); Yang and Ouyang (2021).

For temporal results, we refer the reader to our supplemental video which contains all 4 animations (using filtering *post*-tonemapping and $R = 0$) presented in this paper, as well as additional combinations for one of the scenes. Additional videos covering all combinations can be found on the project website (see Section 4).

As mentioned in the introduction, screen-space accumulation techniques could technically still be used to collect lighting contributions on glossy surfaces. We tried to use the technique by (Kim, 2019) on such surfaces, but failed to get it to match a reference unless increasing the roughness past 0.25, at which point caustics and objects could no longer be distinguished or seen in the reflections and the mirrors.

5 CONCLUSION

Conclusion. In this paper we presented a new algorithm for real-time rendering of detailed caustics

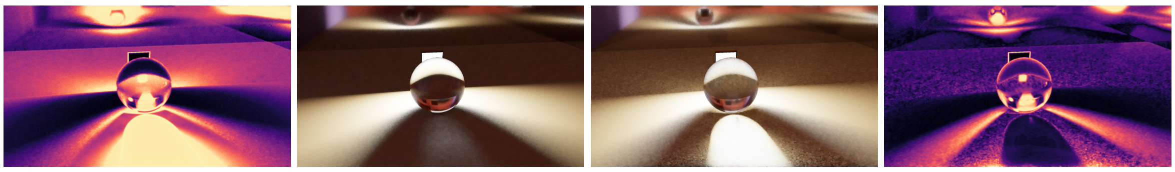

Figure 6: Unlike path tracing, our approach samples the caustics sufficiently that they do not disappear when filtering after tonemapping, to improve temporal stability. From left to right: ꟻLIP error map for *Equal Time PT (2 spp)*, Equal Time PT (2 spp), OurTemporal, ꟻLIP error map for *OurTemporal*. These can be compared to the reference image and results obtained when filtering prior to tonemapping that are found in Table 2.

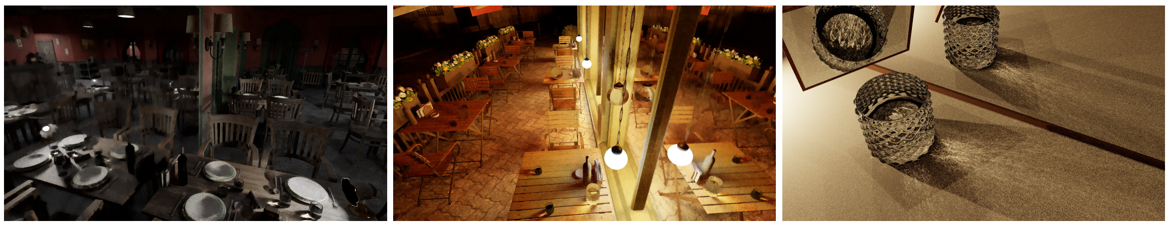

Figure 7: Our approach can be applied to more complex scenes (left image: 39 ms, path length of 7 segments; centre image: 46 ms, path length of 6 segments) and scales to more intricate caustics (right image, 1 s, path length of 6 segments; 175k spp for an equal quality path tracer). For the first two images, the main costs are path tracing (17–19 ms), light tracing (8–11 ms), and AS re-build (6 ms). All three images were rendered using our temporal version, and while the first two were filtered with SVGF, the last was accumulated over multiple frames.

appearing in long specular view paths. Our method makes use of recent hardware-accelerated ray tracing for both view and light rays, and for BVH construction. We create a temporal cache of previous frame light intensity to improve temporal filtering. Temporal filtering costs more in frame time, if not performed asynchronously, but improves image quality in most cases. Our results show that performance of 20–28 ms for the *box* scenes, is possible with temporal filtering for scenes with reflective surfaces showing caustics that are not rendered by existing screen-space accumulation techniques. Additionally, our approach can be applied to complex scenes.

Future work. The variation in collection point locations from frame to frame depending on the material sampling goes against the assumptions made by current BVH refitting approaches, resulting in low tracing performance. Temporal filtering of caustics remains an open issue with one of its challenges being the obtention of motion vectors for the caustics, which would help in reducing ghosting artefacts. The data cached by our approach could be extended to include, for example, a reservoir to use ReSTIR (Bitterli et al., 2020) even on surfaces visible via mirror(s).

ACKNOWLEDGMENTS

We thank Jacob Munkberg for valuable insights and discussions. Pierre Moreau was supported by Vetenskapsrådet, and Michael Doggett is supported by ELLIIT and WASP. The transparent glass used in the teaser and Figure 7 was made by Simon Wendsche[2]. The *Bistro Interior* and *Bistro Exterior* scenes used in Figure 7 are courtesy of Amazon Lumberyard (2017).

REFERENCES

Akenine-Möller, T., Crassin, C., Boksansky, J., Belcour, L., Panteleev, A., and Wright, O. (2021). Improved shader and texture level of detail using ray cones. *Journal of Computer Graphics Techniques (JCGT)*, 10(1):1–24.

Amazon Lumberyard (2017). Amazon Lumberyard bistro, open research content archive (ORCA). http://developer.nvidia.com/orca/amazon-lumberyard-bistro.

Andersson, P., Nilsson, J., Akenine-Möller, T., Oskarsson, M., Åström, K., and Fairchild, M. D. (2020). ꟻLIP: A Difference Evaluator for Alternating Images. *Proceedings of the ACM on Computer Graphics and Interactive Techniques*, 3(2):15:1–15:23.

Arvo, J. (1986). Backward ray tracing. In *Developments in Ray Tracing (SIGGRAPH 86 Course Notes)*, volume 12.

Benty, N., Yao, K.-H., Clarberg, P., Chen, L., Kallweit, S., Foley, T., Oakes, M., Lavelle, C., and Wyman, C. (2020). The Falcor rendering framework. https://github.com/NVIDIAGameWorks/Falcor.

Bitterli, B., Wyman, C., Pharr, M., Shirley, P., Lefohn, A.,

[2]https://byob.carbonmade.com/

and Jarosz, W. (2020). Spatiotemporal reservoir resampling for real-time ray tracing with dynamic direct lighting. *ACM Trans. Graph.*, 39(4).

Evangelou, I., Papaioannou, G., Vardis, K., and Vasilakis, A. A. (2021). Fast radius search exploiting ray tracing frameworks. *Journal of Computer Graphics Techniques (JCGT)*, 10(1):25–48.

Gruen, H. (2019). Ray-guided volumetric water caustics in single scattering media with dxr. In *Ray Tracing Gems: High-Quality and Real-Time Rendering with DXR and Other APIs*, chapter 14, pages 183–201. Apress, Berkeley, CA.

Hachisuka, T., Ogaki, S., and Jensen, H. W. (2008). Progressive photon mapping. In *ACM SIGGRAPH Asia 2008 Papers*, SIGGRAPH Asia '08, New York, NY, USA. Association for Computing Machinery.

Heckbert, P. S. (1990). Adaptive radiosity textures for bidirectional ray tracing. *SIGGRAPH Comput. Graph.*, 24(4):145–154.

Hu, W. and Qin, K. (2007). Interactive approximate rendering of reflections, refractions, and caustics. *IEEE Transactions on Visualization and Computer Graphics*, 13(1):46–57.

Igehy, H. (1999). Tracing ray differentials. In *Proceedings of the 26th Annual Conference on Computer Graphics and Interactive Techniques*, SIGGRAPH '99, page 179–186, USA. ACM Press/Addison-Wesley Publishing Co.

Jensen, H. W. (2001). *Realistic Image Synthesis Using Photon Mapping*. A. K. Peters.

Kim, H. (2019). Caustics using screen-space photon mapping. In Haines, E. and Akenine-Möller, T., editors, *Ray Tracing Gems: High-Quality and Real-Time Rendering with DXR and Other APIs*, chapter 30, pages 543–555. Apress, Berkeley, CA.

McGuire, M. and Luebke, D. (2009). Hardware-accelerated global illumination by image space photon mapping. In *Proceedings of the Conference on High Performance Graphics 2009*, HPG '09, page 77–89, New York, NY, USA. Association for Computing Machinery.

Ouyang, Y. and Yang, X. (2020a). Generating ray-traced caustic effects in unreal engine 4, part 1. https://developer.nvidia.com/blog/generating-ray-traced-caustic-effects-in-unreal-engine-4-part-1/.

Ouyang, Y. and Yang, X. (2020b). Generating ray-traced caustic effects in unreal engine 4, part 2. https://developer.nvidia.com/blog/generating-ray-traced-caustic-effects-in-unreal-engine-4-part-2/.

Schied, C., Kaplanyan, A., Wyman, C., Patney, A., Chaitanya, C. R. A., Burgess, J., Liu, S., Dachsbacher, C., Lefohn, A., and Salvi, M. (2017). Spatiotemporal variance-guided filtering: Real-time reconstruction for path-traced global illumination. In *Proceedings of High-Performance Graphics*, HPG '17, New York, NY, USA. Association for Computing Machinery.

Shah, M. A., Konttinen, J., and Pattanaik, S. (2007). Caustics mapping: An image-space technique for real-time caustics. *IEEE Transactions on Visualization and Computer Graphics*, 13(2):272–280.

Szirmay-Kalos, L., Aszódi, B., Lazányi, I., and Premecz, M. (2005). Approximate ray-tracing on the gpu with distance impostors. *Computer Graphics Forum*, 24(3):695–704.

Wald, I., Usher, W., Morrical, N., Lediaev, L., and Pascucci, V. (2019). RTX Beyond Ray Tracing: Exploring the Use of Hardware Ray Tracing Cores for Tet-Mesh Point Location. In *High-Performance Graphics - Short Papers*.

Wang, X. and Zhang, R. (2021). Rendering transparent objects with caustics using real-time ray tracing. *Computers & Graphics*, 96:36–47.

Wyman, C. and Davis, S. (2006). Interactive image-space techniques for approximating caustics. In *Proceedings of the 2006 Symposium on Interactive 3D Graphics and Games*, I3D '06, page 153–160, New York, NY, USA. Association for Computing Machinery.

Wyman, C. and Nichols, G. (2009). Adaptive caustic maps using deferred shading. *Computer Graphics Forum*, 28(2):309–318.

Yang, X. and Ouyang, Y. (2021). Real-time ray traced caustics. In *Ray Tracing Gems II*, chapter 30, pages 469–497. Apress, Berkeley, CA.

Zeng, Z., Liu, S., Yang, J., Wang, L., and Yan, L.-Q. (2021). Temporally reliable motion vectors for real-time ray tracing. *Computer Graphics Forum*, 40(2).